Parametric Control of a Superconducting Flux Qubit

S. Saito,[1,2] T. Meno,[3] M. Ueda,[1,2,4] H. Tanaka,[1,2] K. Semba,[1,2] and H. Takayanagi[1,2]

[1]*NTT Basic Research Laboratories, NTT Corporation, Atsugi, Kanagawa 243-0198, Japan*
[2]*CREST, Japan Science and Technology Agency, Kawaguchi, Saitama 332-0012, Japan*
[3]*NTT Advanced Technology Corporation, Atsugi, Kanagawa 243-0198, Japan*
[4]*Department of Physics, Tokyo Institute of Technology, Meguro, Tokyo 152-8551, Japan*

(Received 16 July 2005; revised manuscript received 23 December 2005; published 13 March 2006)

Parametric control of a superconducting flux qubit has been achieved by using two-frequency microwave pulses. We have observed Rabi oscillations stemming from parametric transitions between the qubit states when the sum of the two microwave frequencies or the difference between them matches the qubit Larmor frequency. We have also observed multiphoton Rabi oscillations corresponding to one- to four-photon resonances by applying single-frequency microwave pulses. The parametric control demonstrated in this work widens the frequency range of microwaves for controlling the qubit and offers a high quality testing ground for exploring nonlinear quantum phenomena of macroscopically distinct states.

DOI: 10.1103/PhysRevLett.96.107001 PACS numbers: 74.50.+r, 03.67.Lx, 42.50.Hz, 85.25.Dq

Quantum-state engineering has become one of the most important arenas in quantum physics. In particular, the coherent control of quantum two-state systems (TSS), which are applicable to quantum bits (qubits), has attracted increasing interest in the context of quantum computing and quantum information processing [1]. Various candidate physical systems are being studied for the future implementation of qubits. These include artificial quantum TSS like superconducting qubits [2–9] as well as naturally existing quantum TSS like nuclear spins [10,11]. Of the many candidates that may enable us to realize quantum computation, superconducting qubits based on Josephson junctions have gained increasing importance because of their potential controllability and scalability.

The coherent control of a single qubit has been demonstrated in many types of superconducting circuits, such as charge [2], charge-phase [3], phase [4,5], and flux qubits [7–9]. Recently, two-qubit operation has been demonstrated in charge [12] and phase qubits [13]. In addition to qubit operation, the superconducting qubit offers a testing ground for exploring interactions between photons and artificial macroscopic objects, which we shall refer to as ''atoms.'' In the weak-driving limit, the interaction between a single atom and a single microwave photon has been demonstrated with a charge qubit, which is strongly coupled to a superconducting transmission line resonator [14]. In the strong-driving regime, superconducting qubits have exhibited nonlinear optical responses: multiphoton Rabi oscillations have been observed in a charge qubit by using microwave pulses [15], and under continuous microwave irradiation, multiphoton absorption has been observed in a phase [16] and a flux qubit [17].

In this Letter, we describe the parametric control of *macroscopically distinct states* [18] in a superconducting flux qubit with two-frequency microwave pulses. We have succeeded in observing two-photon Rabi oscillations of the qubit caused by a parametric transition when the qubit Larmor frequency matches either the sum of the two microwave frequencies or the difference between them. We also show multiphoton Rabi oscillations corresponding to one- to four-photon resonances under single-frequency microwave pulse irradiation where the qubit Larmor frequency was equal to multiples of the microwave frequency. The parametric and multiphoton transitions clearly exhibit high nonlinearity due to interactions between a single atom and microwaves.

If we are to observe highly nonlinear phenomena in superconducting qubits with strong microwave driving, the electromagnetic environment of the qubits must be well controlled because the strong driving easily excites unwanted environmental resonances, which destroy the qubit coherence. Our device was fabricated using electron beam lithography and shadow evaporation techniques defining an inner aluminum loop forming the qubit and an outer loop enclosing the dc-SQUID loop used for the readout [Fig. 1(a)]. The inner loop contains three Josephson junctions, one with an area $\alpha \simeq 0.8$ times smaller than the nominally identical area of the other two with critical current $I_c \approx 430$ nA. The outer loop comprises two Josephson junctions of critical current ≈ 140 nA. We placed an on-chip microwave line close to the qubit at a distance of 20 μm so that the qubit could be strongly driven by oscillating magnetic fields, which are induced by microwave currents flowing through the line. To control the electromagnetic environment surrounding the qubit, we put resistors R_{I1} and R_{V1}, lead inductances L, and shunt capacitors C and $2C$ on the chip [Fig. 1(b)]. The resistors damp unwanted resonances, which are generated in, for example, leads and parasitic capacitors outside the resistors. There are two well-controlled resonance modes that are produced in the circuits inside the resistors, namely, the on-chip components close to the qubit. One is the dc-SQUID's plasma mode with a frequency of 1.0 GHz, which is formed in the two symmetrical loops, each being com-

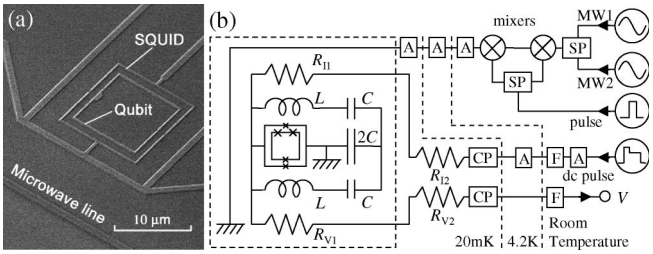

FIG. 1. (a) Scanning electron micrograph of a flux qubit (inner loop) and a dc-SQUID (outer loop). The loop sizes of the qubit and SQUID are $10.2 \times 10.4\ \mu\text{m}^2$ and $12.6 \times 13.5\ \mu\text{m}^2$, respectively. They are magnetically coupled by the mutual inductance $M \approx 13$ pH. (b) A circuit diagram of the flux qubit measurement system. On-chip components are shown in the dashed box. $L \approx 140$ pH, $C \approx 9.7$ pF, $R_{I1} = 0.9\ \text{k}\Omega$, $R_{V1} = 5\ \text{k}\Omega$. Surface mount resistors $R_{I2} = 1\ \text{k}\Omega$ and $R_{V2} = 3\ \text{k}\Omega$ are set in the sample holder. We put adequate copper powder filters CP and LC filters F and attenuators A for each line.

posed of L, C, $2C$, and the SQUID's Josephson inductance. The other is the harmonic LC resonance mode with a frequency of 4.311 GHz, which is produced in the larger loop consisting of the two L's and the two C's. In this way, we have achieved an artificial TSS in a well-controlled environment.

The three Josephson junctions of the qubit form a double-well potential in the space of the Josephson phase when about half a flux quantum threads the qubit loop. We use the two lowest levels in the potential as the qubit states, which are well separated from the higher levels. Thus, the qubit is described by the Hamiltonian $H_{\text{qb}} = (\hbar/2)(\varepsilon\sigma_z + \Delta\sigma_x)$, where $\sigma_{x,z}$ are the Pauli spin matrices. The eigenstates of σ_z describe clockwise and counter-clockwise persistent currents in the qubit. The qubit tunnel splitting is described by $\hbar\Delta$, and $\hbar\varepsilon = 2I_{\text{p}}\Phi_0(\Phi_{\text{qb}}/\Phi_0 - 1.5)$ is the energy imbalance between the two potential wells caused by the externally applied magnetic flux threading the qubit loop Φ_{qb}, where $\Phi_0 = h/2e$ is the flux quantum and $I_{\text{p}} = I_{\text{c}}\sqrt{1 - (1/2\alpha)^2}$ is the magnitude of the qubit persistent current when the qubit is in the σ_z eigenstates and I_{c} is the critical current of the larger junctions. The energy difference between the ground state $|\text{g}\rangle$ and the first excited state $|\text{e}\rangle$ of the qubit is $\hbar\omega_{\text{qb}} = hf_{\text{qb}} = \hbar\sqrt{\varepsilon^2 + \Delta^2}$. Assuming that the applied microwaves are in coherent states, we may describe the qubit under microwave irradiation by the Hamiltonian

$$H = \frac{\hbar}{2}(\varepsilon\sigma_z + \Delta\sigma_x) + \sum_{k=1}^{l} 2\hbar g_k \alpha_k \sigma_z \cos\omega_{\text{MW}k} t, \quad (1)$$

where l is one (two) in the case of a single- frequency (two-frequency) microwave and g_k is the coupling between the qubit and the kth microwave (MWk), whose amplitude and frequency are α_k and $f_{\text{MW}k} = \omega_{\text{MW}k}/2\pi$, respectively. Solving the Schrödinger equation with the Hamiltonian (1) without the rotating wave approximation, we obtain the time evolution of the probability $P_{\text{e}}(t)$ with which we find the qubit in $|\text{e}\rangle$. The probability $P_{\text{e}}(t)$ shows a periodic oscillation, namely, Rabi oscillation, under resonant conditions $\omega_{\text{qb}} = n_1\omega_{\text{MW1}}$ (for the single-frequency microwave) or $\omega_{\text{qb}} = |n_1\omega_{\text{MW1}} \pm n_2\omega_{\text{MW2}}|$ (for the two-frequency microwave), where n_k is the MWk photon number. When $\varepsilon = 0$, the frequency of the single-photon Rabi oscillation shows its well-known linear dependence on the microwave amplitude, $\Omega_{\text{Rabi}} = 2g_1\alpha_1$. In contrast, when $\varepsilon \neq 0$, the oscillation frequency is given for single-frequency microwave irradiation by

$$\Omega_{\text{Rabi}} = \frac{\Delta}{A} J_{n_1}\left(A\frac{4g_1\alpha_1}{\omega_{\text{MW1}}}\right) \quad (2)$$

and for the two-frequency microwave irradiation by

$$\Omega_{\text{Rabi}} = \frac{\Delta}{A} J_{n_1}\left(A\frac{4g_1\alpha_1}{\omega_{\text{MW1}}}\right) J_{n_2}\left(A\frac{4g_2\alpha_2}{\omega_{\text{MW2}}}\right). \quad (3)$$

Here J_{n_k} is the n_kth order Bessel function of the first kind and $A \equiv \varepsilon/\omega_{\text{qb}} \approx 1$. This approximation is valid when $\varepsilon \gg \Delta$. The dressed atom approach gives results similar to Eq. (2) [15,19].

The measurements were carried out in a dilution refrigerator. The sample was mounted in a gold plated copper box that was thermalized to the base temperature of 20 mK ($k_{\text{B}}T \ll \hbar\omega_{\text{qb}}$). To produce two-frequency microwave pulses, we added two microwaves MW1 and MW2 with frequencies of f_{MW1} and f_{MW2}, respectively, by using a splitter SP [Fig. 1(b)]. Then we shaped them into microwave pulses through two mixers. We measured the amplitude of MWk $V_{\text{MW}k}$ at the point between the attenuator and the mixer with an oscilloscope. We confirmed that unwanted higher-order frequency components in the pulses, for example, $|f_{\text{MW1}} \pm f_{\text{MW2}}|$, $2f_{\text{MW1}}$, and $2f_{\text{MW2}}$ are negligibly small under our experimental conditions. First, we choose the operating point by setting Φ_{qb} around $1.5\Phi_0$, which fixes the qubit Larmor frequency f_{qb}. The qubit is thermally initialized to be in $|\text{g}\rangle$ by waiting for 300 μs, which is much longer than the qubit energy relaxation time (for example 3.8 μs at $f_{\text{qb}} = 11.1$ GHz). Then a qubit operation is performed by applying a microwave pulse to the qubit. The pulse, with an appropriate length t_{p}, amplitudes $V_{\text{MW}k}$, and frequencies $f_{\text{MW}k}$, prepares a qubit in the superposition state of $|\text{g}\rangle$ and $|\text{e}\rangle$. After the operation, we immediately apply a dc readout pulse to the dc-SQUID. This dc pulse consists of a short (70 ns) initial pulse followed by a long (1.5 μs) trailing plateau that has 0.6 times the amplitude of the initial part. For $\Phi_{\text{qb}} < 1.5\Phi_0$, if the qubit is detected as being in $|\text{e}\rangle$, the SQUID switches to a voltage state and an output voltage pulse should be observed; otherwise there should be no output voltage pulse. By repeating the measurement 8000 times, we obtain the SQUID switching probability P_{sw}, which is

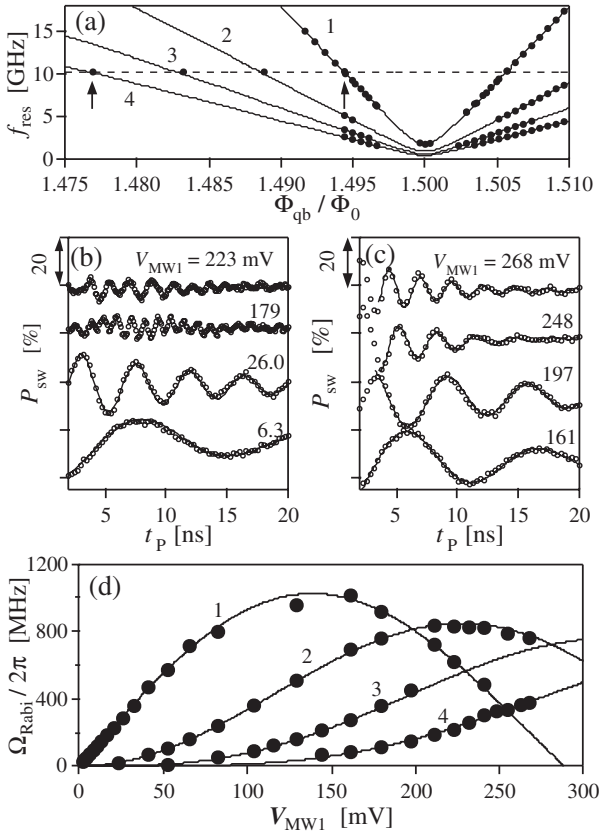

FIG. 2. Experimental results with single-frequency microwave pulses. (a) Spectroscopic data of the qubit. Each set of the dots represents the resonant frequencies f_{res} caused by the one- to four-photon absorption processes. The solid curves are numerical fits. The dashed line shows a microwave frequency f_{MW1} of 10.25 GHz. (b) One-photon Rabi oscillations of P_{sw} with exponentially damped oscillation fits. Both the qubit Larmor frequency f_{qb} and the microwave frequency f_{MW1} are 10.25 GHz. The external flux is $\Phi_{qb}/\Phi_0 = 1.4944$. (c) Four-photon Rabi oscillations when $f_{qb} = 41.0$ GHz, $f_{MW1} = 10.25$ GHz, and $\Phi_{qb}/\Phi_0 = 1.4769$. (d) The microwave amplitude dependence of the Rabi frequencies $\Omega_{Rabi}/2\pi$ up to four-photon Rabi oscillations. The solid curves represent theoretical fits.

directly related to $P_e(t_p)$ for the dc readout pulse with a proper amplitude. For $\Phi_{qb} > 1.5\Phi_0$, P_{sw} is directly related to $1 - P_e(t_p)$.

We performed a spectroscopy measurement of the qubit with long (50 ns) single-frequency microwave pulses. We observed multiphoton resonant peaks ($\Phi_{qb} < 1.5\Phi_0$) and dips ($\Phi_{qb} > 1.5\Phi_0$) in the dependence of P_{sw} on f_{MW1} at a fixed magnetic flux Φ_{qb}. We obtained the qubit energy diagram by plotting their positions as a function of Φ_{qb}/Φ_0 [Fig. 2(a)]. We took the data around the degeneracy point $\Phi_{qb} \approx 1.5\Phi_0$ by applying an additional dc pulse to the microwave line to shift Φ_{qb} away from $1.5\Phi_0$ just before the readout, because the dc-SQUID could not distinguish the qubit states around the degeneracy point. The top solid curve in Fig. 2(a) represents a numerical fit to the resonant frequencies of one-photon absorption. From this fit, we obtain the qubit parameters $E_J/h = 213$ GHz, $\Delta/2\pi = 1.73$ GHz, and $\alpha = 0.8$. The other curves in Fig. 2(a) are drawn by using these parameters for $n_1 = 2$, 3, and 4.

Next, we used short single-frequency microwave pulses with a frequency of 10.25 GHz to observe the coherent quantum dynamics of the qubit. Figs. 2(b) and 2(c) show one- and four-photon Rabi oscillations observed at the operating points indicated by arrows in Fig. 2(a) with various microwave amplitudes V_{MW1}. These data can be fitted by damped oscillations $\propto \exp(-t_p/T_d)\cos(\Omega_{Rabi}t_p)$, except for the upper two curves in Fig. 2(b). Here, t_p and T_d are the microwave pulse length and qubit decay time, respectively. To obtain Ω_{Rabi}, we performed a fast Fourier transform on the curves that we could not fit by damped oscillations. The strong microwave irradiation with the frequency of 10.25 GHz excited many levels of the harmonic LC resonance mode at 4.311 GHz although the frequencies were very different. We believe that these excitations degraded the Rabi oscillations in the higher V_{MW1} range of Fig. 2(b). Numerical simulations reproduced these phenomena qualitatively. Figure 2(d) shows the V_{MW1} dependences of $\Omega_{Rabi}/2\pi$ up to four-photon Rabi oscillations, which are well reproduced by Eq. (2). Here, we used only one scaling parameter $a(10.25\ \text{GHz}) = 13\ \text{V}^{-1}$ defined as $a(f_{MW1}) \equiv 4g_1\alpha_1/\omega_{MW1}V_{MW1}$, because it is hard to measure the real amplitude of the microwave applied to the qubit at the sample position. The scaling parameter $a(f_{MW1})$ reflects the way in which the applied microwave is attenuated during its transmission to the qubit and the efficiency of the coupling between the qubit and the on-chip microwave line. In this way, we can estimate the real microwave amplitude and the interaction energy between the qubit and the microwave $2\hbar g_1\alpha_1$ by fitting the dependence of $\Omega_{Rabi}/2\pi$ on V_{MW1}. These results show that we can reach a driving regime that is so strong that the interaction energy $2\hbar g_1\alpha_1$ is larger than the qubit transition energy $\hbar\omega_{qb}$.

We have also performed experiments with two microwave frequencies f_{MW1} and f_{MW2}. First, we carry out a spectroscopy measurement by using long (50 ns) two-frequency microwave pulses. In addition to resonances caused by the multiphoton absorption processes at multiples of each microwave frequency ($f_{qb} = n_1 f_{MW1}$, $n_2 f_{MW2}$), we also clearly observe those due to parametric processes ($f_{qb} = |f_{MW1} \pm f_{MW2}|$) (not shown).

We next investigate the coherent oscillations of the qubit through the parametric processes by using short two-frequency microwave pulses. Figure 3(a) [Fig. 3(b)] shows the Rabi oscillations of P_{sw} when the qubit Larmor frequency $f_{qb} = 26.45$ (7.4) GHz corresponds to the sum of the two microwave frequencies $f_{MW1} = 16.2$ GHz and $f_{MW2} = 10.25$ GHz (the difference between $f_{MW1} = 11.1$ GHz and $f_{MW2} = 18.5$ GHz) and the microwave am-

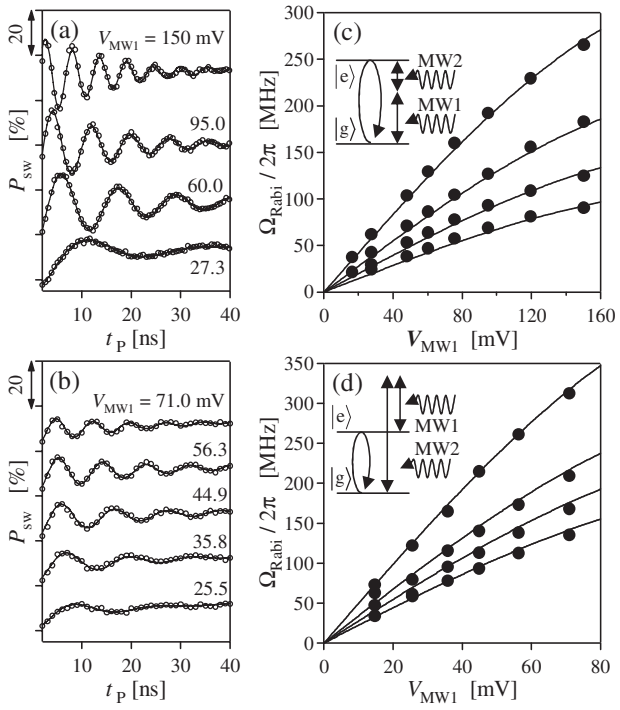

FIG. 3. Experimental results with two-frequency microwave pulses. (a) [(b)] Two-photon Rabi oscillations due to a parametric process when $f_{qb} = f_{MW2} + (-)f_{MW1}$. The solid curves are fits by exponentially damped oscillations. (c) [(d)] Rabi frequencies as a function of V_{MW1}, which are obtained from the data in Figs. 3(a) and 3(b). The dots represent experimental data when $V_{MW2} = 16.9$, 23.5, 33.0, and 52.0 (50.1, 62.9, 79.1, and 124.7) mV from the bottom set of dots to the top one. The solid curves represent Eq. (3). The inset is a schematic of the parametric process that causes two-photon Rabi oscillation when $f_{qb} = f_{MW2} + (-)f_{MW1}$.

plitude of MW2 V_{MW2} was fixed at 33.0 (50.1) mV. They are well fitted by exponentially damped oscillations $\propto \exp(-t_p/T_d)\cos(\Omega_{Rabi}t_p)$. The Rabi frequencies obtained from the data in Figs. 3(a) and 3(b) are well reproduced by Eq. (3) without any fitting parameters [Figs. 3(c) and 3(d), respectively]. Here, we use Δ, which was obtained from the spectroscopy measurement [Fig. 2(a)] and use $a(10.25\ \text{GHz}) = 13\ \text{V}^{-1}$ and $a(16.2\ \text{GHz}) = 7.4\ \text{V}^{-1}$ [$a(11.1\ \text{GHz}) = 13\ \text{V}^{-1}$ and $a(18.5\ \text{GHz}) = 8.2\ \text{V}^{-1}$], which were obtained from Rabi oscillations by using single-frequency microwave pulses with each frequency. Those results provide strong evidence that we can achieve parametric control of the qubit with two-frequency microwave pulses.

In summary, we have investigated the nonlinear responses of macroscopically distinct states in a superconducting flux qubit. First, we observed multiphoton Rabi oscillations caused by up to four-photon transitions by using single-frequency microwave pulses. Next, we successfully demonstrated parametric control of the qubit by using two-frequency microwave pulses. We observed Rabi oscillations of the qubit caused by parametric transitions when $f_{qb} = |f_{MW1} \pm f_{MW2}|$. The microwave amplitude dependences of the Rabi frequencies are well reproduced by Bessel functions derived from a semiclassical model. These results indicate that the flux qubit offers a good testing ground for exploring quantum nonlinear phenomena in a macroscopic quantum object. Furthermore, these multiphoton processes observed in our experiment widen the frequency range of microwaves for controlling flux qubits. By utilizing the parametric processes, we can control qubits with much higher frequencies than the qubit Larmor frequency. This implies that we can filter out the noise around and lower than the qubit frequency from the microwave line by using a high-pass filter. This will greatly improve the qubit coherence.

We thank T. Kutsuzawa, F. Deppe for useful discussions and for help with the experimental setup. We also acknowledge useful discussions with J. Johansson, H. Nakano, M. Thorwart, Y. Yamamoto, J. E. Mooij, C. J. P. M. Harmans, and Y. Nakamura. This work was supported by a CREST program of the Japan Science and Technology Agency (JST). M. U. acknowledges support by an ERATO program of JST.

[1] M. A. Nielsen and I. L. Chuang, *Quantum Computation and Quantum Information* (Cambridge University Press, Cambridge, 2000).
[2] Y. Nakamura, Y. A. Pashkin, and J. S. Tsai, Nature (London) **398**, 786 (1999).
[3] D. Vion *et al.*, Science **296**, 886 (2002).
[4] Y. Yu, S. Han, X. Chu, S.-I. Chu, and Z. Wang, Science **296**, 889 (2002).
[5] J. M. Martinis, S. Nam, J. Aumentado, and C. Urbina, Phys. Rev. Lett. **89**, 117901 (2002).
[6] J. E. Mooij *et al.*, Science **285**, 1036 (1999).
[7] I. Chiorescu, Y. Nakamura, C. J. P. M. Harmans, and J. E. Mooij, Science **299**, 1869 (2003).
[8] T. Kutsuzawa *et al.*, Appl. Phys. Lett. **87**, 073501 (2005).
[9] B. L. T. Plourde *et al.*, Phys. Rev. B **72**, 060506(R) (2005).
[10] L. M. K. Vandersypen *et al.*, Nature (London) **414**, 883 (2001).
[11] G. Yusa, K. Muraki, K. Hashimoto, and Y. Hirayama, Nature (London) **434**, 1001 (2005).
[12] T. Yamamoto, Y. A. Pashkin, O. Astafiev, Y. Nakamura, and J. S. Tsai, Nature (London) **425**, 941 (2003).
[13] R. McDermott *et al.*, Science **307**, 1299 (2005).
[14] A. Wallraff *et al.*, Nature (London) **431**, 162 (2004).
[15] Y. Nakamura, Y. A. Pashkin, and J. S. Tsai, Phys. Rev. Lett. **87**, 246601 (2001).
[16] A. Wallraff, T. Duty, A. Lukashenko, and A. V. Ustinov, Phys. Rev. Lett. **90**, 037003 (2003).
[17] S. Saito *et al.*, Phys. Rev. Lett. **93**, 037001 (2004).
[18] A. J. Leggett, J. Phys. Condens. Matter **14**, R415 (2002).
[19] C. Cohen-Tannoudji, J. Dupont-Roc, and G. Grynberg, *Atom-Photon Interactions* (Wiley, New York, 1992).